

1 **Tectonic strain recorded by magnetic fabrics (AMS) in plutons, including Mt**
2 **Kinabalu, Borneo: A tool to explore past tectonic regimes and syn-magmatic**
3 **deformation**

4

5 Burton-Johnson, A^{a*}, Macpherson, C.G.^b, Muraszko, J.R.^c, Harrison, R.J.^c, and Jordan,
6 T.A.^a

7

8 ^aBritish Antarctic Survey, High Cross, Madingley Road, Cambridge, CB3 0ET, UK

9 ^bDepartment of Earth Sciences, University of Durham, Durham, DH1 3LE, UK

10 ^cDepartment of Earth Sciences, University of Cambridge, Cambridge, CB2 3EQ, UK

11 *Author for correspondence

12 E-mail: alerto@bas.ac.uk

13 Tel. +44 (0)1223 221284

14 Keywords: Tectonics; Magnetic fabrics; Magmatic fabrics; Intrusions; Granites; SE
15 Asia; Mt Kinabalu

16 **Highlights**

17 (1) The tectonic fabric in the AMS data of Mt Kinabalu, Borneo, reveals Miocene
18 extension in SE Asia between 7.9-7.3 Ma (later than previously recognised).
19 Correcting for paleomagnetic rotation, extension was oriented NW-SE at
20 $319^\circ \pm 13.1^\circ$.

21 (2) Tectonic strain fabrics are far more ubiquitous in global plutonic fabrics
22 than previously recognised.

23 (3) AMS determination of tectonic strain in dated plutons is a powerful tool for
24 determining past tectonics within a temporal framework, particularly
25 when combined with evidence for paleomagnetic rotation.

26 **Abstract**

27 Tectonic strain commonly overprints magmatic fabrics in AMS (Anisotropy of
28 Magnetic Susceptibility) data for plutonic rocks produced by both compressional
29 and extensional regimes. Mt Kinabalu, Borneo, is a composite pluton with an
30 exceptional vertical range of exposure and clearly defined internal contacts. We
31 show that tectonic fabrics are recorded pervasively throughout the intrusion, even
32 near contacts, and present a workflow distinguishing compressive and
33 extensional syn-magmatic deformation. At Mt Kinabalu this reveals a pervasive
34 tectonic fabric indicating NW-SE Miocene extension in Borneo at 7.9-7.3 Ma, later
35 than previously recognised, oriented NW-SE at $319^{\circ} \pm 13.1^{\circ}$. Comparing data from
36 Mt Kinabalu with data from globally distributed studies shows that tectonic strain
37 is commonly recorded by plutons. Therefore, AMS fabric can be used to identify
38 the syn-magmatic tectonic setting and combined with both geochronology and
39 evidence for paleomagnetic rotation to provide a powerful tool for accurate
40 determination of syn-magmatic tectonic regimes and strain orientations within
41 temporal frameworks.

42

43 **1. Introduction**

44 Determining syn-magmatic strain is a challenge for research into plutonic
45 intrusions because traditional structural evidence (faults and dykes) can only
46 record the post-magmatic deformation of their host pluton. Instead, evidence is
47 obtained from mineral fabric alignment (Hutton, 1988; Pitcher, 1997; Paterson et
48 al., 1998; Schofield and D'Lemos, 1998). Be this visible alignment of the rock-
49 forming phases, or more subtle alignment of the magnetically susceptible phases,
50 the recorded strain results from combined magmatic, tectonic, and lithostatic
51 stresses during crystallisation.

52 Identifying the effects of magmatic or tectonic strain provides valuable
53 information. For example, a magma flow fabric would inform how plutons are
54 intruded, whilst a tectonic fabric would record the tectonic strain orientation
55 during emplacement. However, contrasting interpretations of plutonic mineral
56 fabrics as the recorders of magmatic flow or tectonic strain exist, even for similar
57 intrusions and tectonic settings (e.g. Petronis and O'Driscoll, 2013; Tomek et al.,
58 2016).

59 In this study we use field and magnetic fabric (AMS, Anisotropy of Magnetic
60 Susceptibility) data from the Mt Kinabalu intrusion of Borneo to demonstrate the
61 pervasive overprint of tectonic fabrics upon magmatic fabrics.. We use the Mt
62 Kinabalu intrusion to demonstrate that determining these tectonic fabrics by AMS
63 offers a powerful tool to obtain temporal constraints on past tectonic regimes. In
64 this case, we constrain the syn-magmatic deformation during a period of disputed
65 tectonics in SE Asia. We compare this with data from other globally distributed
66 plutons to show that such records of deformation are commonly present in
67 granitic plutons,

68 **2. Application of AMS to mineral fabric research**

69 Mineral fabrics in granitic plutons have long been mapped and studied but
70 accurate determinations of these fabrics are often difficult and observations risk
71 being biased by the two dimensional nature of an outcrop. Consequently, analysis
72 of the Anisotropy of Magnetic Susceptibility (AMS) has frequently been applied to
73 granitic intrusions (Bouchez, 1997). This method measures variation in the

74 susceptibility of each of the three, principal, magnetic axes of an oriented sample
75 (Ježek and Hrouda, 2004); K1, the axis of maximum magnetic susceptibility; K3,
76 the axis of minimum susceptibility; and K2, the intermediate axis (Fig. 1). This
77 method allows fast, inexpensive, and accurate determination of three-dimensional
78 mineral fabrics even when such fabric cannot be observed in outcrop.

79 Magnetic fabrics can be hosted by ferro-, ferri-, para-, or diamagnetic phases.
80 These classifications and the grain size of the carrier phase determine the nature
81 of observed magnetic fabrics. The magnetic susceptibility of ferro- and
82 ferrimagnetic phases (e.g. magnetite, and pyrrhotite) is three orders of magnitude
83 greater than paramagnetic phases (Hunt et al., 1995). In ferromagnetic minerals
84 all magnetic moments align, whilst in ferrimagnetic minerals some point in the
85 opposite direction. Below their Curie temperature, ferro- and ferrimagnetic
86 phases magnetise when exposed to a magnetic field and remain magnetic once the
87 field is removed. In contrast, the much less magnetic phases exhibiting
88 paramagnetism (e.g. biotite and hornblende) cease being magnetic once the field
89 is removed. The weakest magnetic effect occurs in diamagnetic minerals (e.g.
90 quartz), which are often classed as 'non-magnetic'.

91 Magnetic domains in ferro- and ferrimagnetic phases cause their magnetic
92 susceptibility to be grain size dependent, with larger grains displaying greater
93 susceptibilities (Hunt et al., 1995). As grain size increases the magnetic domain
94 state changes from single-domain to multi-domain. This is important for AMS
95 studies, as whilst the axes of magnetic susceptibility in multi-domain grains (and
96 the paramagnetic phases biotite and amphibole; Bouchez, 1997) correspond with
97 the grain shape, in single-domain grains the magnetic susceptibility axes are
98 inverted (Stephenson et al., 1986), producing inverse magnetic fabrics (Hrouda
99 and Ježek, 2017). Multi- and single-domain grains can be differentiated by varying
100 the temperature and magnetic field imposed on a sample, as in this study.

101 **3. Development of plutonic mineral fabrics**

102 Magmatic mineral fabrics form during crystallisation in response to the stress
103 experienced by partially molten magma until it cools to its solidus. This stress can
104 be a result of: (1) the primary magma flow during emplacement, including stress

105 applied by the ascending magma column on the melt (e.g. Horsman et al., 2005,
106 Stevenson et al., 2006, Stevenson et al., 2007a, Clemens and Benn, 2010); (2)
107 regional tectonic stress during emplacement and crystallisation (e.g. Vigneresse,
108 1995, Benn et al., 1997, Benn, 2009); or (3) a combination of both (e.g.
109 Wennerström and Airo, 1998, Petronis et al., 2012). Whether a plutonic mineral
110 fabric (including AMS) records magmatic or tectonic stresses will be determined
111 by the dominating force during final crystallisation of the pluton at the end of its
112 emplacement.

113 In response to syn-magmatic stress, crystals align their longest principal axis with
114 the long axis of the resultant strain ellipsoid and their shortest principal axis
115 parallel to the short axis of the strain ellipsoid (Fig. 1, Paterson et al., 1998). This
116 relationship of mineral fabric to the strain ellipsoid has been shown by numerical
117 and analogue experiments for simple, non-coaxial shear, for pure, coaxial shear,
118 and for mixed strain conditions (Jeffery, 1922; N. C. Gay, 1968; No C. Gay, 1968;
119 Arbaret et al., 1997; Schulmann et al., 1997; Schulmann and Ježek, 2012).

120 The relationship between stress and strain is complex and requires consideration,
121 as observed magmatic fabrics may record a spectrum from coaxial to non-coaxial
122 deformation. The resultant AMS fabrics expected for different deformation
123 settings are shown in Fig. 2. Coaxial, non-rotational shear can be expected away
124 from rheological contrasts (i.e. away from internal and external contacts),
125 resulting from tectonic stress, and stress exerted by the upwelling magma and
126 overburden (Paterson et al., 1998).

127 Under coaxial, non-rotational shear, the shortest principle axis of the strain
128 ellipsoid is parallel to the direction of maximum compressive stress (σ_1 , Fig. 1 and
129 Fig. 2) whilst the longest principle axis of the strain ellipsoid will be parallel to the
130 direction of minimum compressive stress (σ_3 , Fig. 1 and Fig. 2). The degree to
131 which rigid particles (i.e. the crystal fabric) rotate in response to the strain
132 ellipsoid will increase at higher degrees of strain (N. C. Gay, 1968), increasing the
133 anisotropy of the fabric. However, assuming a random initial particle distribution,
134 even at low degrees of strain the overall distribution of the respective stress and
135 strain axes (and consequently the AMS fabric) will be parallel; albeit with a lower
136 degree of anisotropy (Arbaret et al., 2000).

137 Non-coaxial simple, transpressional, and trans-tensional shearing can be
138 expected to affect both magmatic and tectonic fabrics, particularly where there is
139 differential movement near rheological contrasts. This includes both internal and
140 external contacts (Blumenfeld and Bouchez, 1988; Paterson et al., 1998) or where
141 a pluton is emplaced along a shear zone (Archanjo et al., 1999, 2002).

142 Under non-coaxial shear, with increasing degrees of strain the longest principle
143 axis of the strain ellipsoid (and consequently the crystals) will rotate towards the
144 direction of shearing and consequent stretching (elongation) direction (Fig. 2).
145 The shortest principle axis of the strain ellipsoid and crystals will rotate towards
146 perpendicular to the rheological boundary and orthogonally to the direction of
147 extension (Fig. 2, Arbaret et al., 1997; Benn, 2010). In non-coaxial shear, the
148 relationship between stress and strain orientations is dependent on a number of
149 factors including tectonic setting, the degree of shearing, rheological contrasts and
150 pre-existing structures.

151 As noted, a crystallising melt will experience a spectrum from coaxial to non-
152 coaxial shearing, complicating derivation of stress and strain vectors. However,
153 coaxial and non-coaxial shear produce distinct and different fabrics (Fig. 2). By
154 predicting these fabrics for the magmatic and tectonic strain regimes of a pluton
155 (Fig. 2) and comparing them with the pluton's observed magmatic fabric, the
156 relative contributions of coaxial and non-coaxial shear can be determined.

157 **4. The Mt Kinabalu Intrusion, Borneo**

158 The Mt Kinabalu intrusion of Sabah, Borneo (Fig. 3), provides an ideal field area to
159 investigate magnetic mineral fabrics in three dimensions across a single
160 composite pluton. This is because it has an extensive, glaciated summit; a 2900m
161 vertical range of granitic exposure; clearly mapped internal and external contacts;
162 and strong temporal constraints on the emplacement history. The pluton intruded
163 into the shallow crust (3-12 km, Vogt and Flower, 1989; Cottam et al., 2013;
164 Burton-Johnson et al., 2017) as six major granitic units between 7.85 and 7.55 Ma
165 (Cottam et al., 2010) at the contact between the Mesozoic ophiolitic ultramafic
166 basement (Reinhard and Wenk, 1951; Dhonau and Hutchison, 1965; Koopmans,
167 1967; Kirk, 1968; Leong, 1974) and overlying Eocene to Lower Miocene turbiditic

168 sandstones of the Crocker Formation (Collenette, 1965; van Hattum et al., 2006).
169 Contrasting geodynamic settings have been proposed for NW Borneo at this time,
170 either as a zone of regional compression (Hutchison, 2000; Swauger et al., 2000;
171 King et al., 2010; Pubellier and Morley, 2013) or regional extension (Cottam et al.,
172 2013; Hall, 2013; Burton-Johnson et al., 2017). Contact metamorphism of the
173 adjacent ultramafic rocks generated talc and anthophyllite, indicative of granitoid
174 emplacement at 630-700°C and 2–3 kbar (7-11 km, Bucher and Grapes, 2011).

175 Recent work (Cottam et al., 2010; Burton-Johnson et al., 2017) has shown that the
176 composite pluton was initially emplaced from the top down in a broadly laccolithic
177 structure (Fig. 3C) through upward deformation of the host rocks. Consequently,
178 the oldest unit (the Alexandra Tonalite/Granodiorite, 7.85 ± 0.08 Ma) overlies the
179 subsequent, larger units (the Low's Granite, 7.69 ± 0.07 Ma, and the King Granite,
180 7.46 ± 0.08 Ma). The smaller, vertical planar Donkey Granite (7.49 ± 0.03 Ma)
181 intruded the King Granite before the latter could fully crystallise, producing
182 contacts that vary from gradational to mingled. The final two porphyritic units
183 (the Paka Porphyritic Granite, 7.32 ± 0.09 Ma, and the Mesilau Porphyritic Granite,
184 7.22 ± 0.07 Ma) deviate from the laccolith model having been emplaced laterally
185 and around the periphery of earlier units (Fig. 3c).

186 Mineralogies of the units are summarised in Table 1. Petrographically the units
187 are largely classified as granites (Burton-Johnson et al., 2017), although their
188 major element composition is largely granodiorite (Burton-Johnson et al., in
189 review). Hornblende is the dominant mafic phase in all units except the Alexandra
190 Tonalite/Granodiorite, in which biotite dominates. Visible mineral macrofabrics
191 are absent in all units except the Alexandra unit, in which a biotite foliation was
192 observed, dipping ~ 40 - 60° towards the south-west (Burton-Johnson et al., 2017).
193 To test this observation, image analysis (adapting the methodology of Grove and
194 Jerram, 2011) was conducted on thin sections of each unit (Fig. 4), characterising
195 the colour palettes for biotite and hornblende in each section to determine the 2D
196 orientation of the ferromagnesian crystals (Fig. 4). The standardised resultant
197 vector length, \bar{R} , (the data distribution parameter in circular directional statistics,
198 Davis 1986) is higher (i.e. more consistently distributed) for the Alexandra unit
199 than the later units for both hornblende (0.008 compared to 0.002) and biotite

200 (0.004 compared to 0.002). Furthermore, no microstructural evidence for
201 shearing was observed in the thin sections of any unit (Fig. 4).

202 **5. Methodology**

203 Whilst the glaciated summit of Mt Kinabalu provides complete exposure, and the
204 topography provides an exceptional vertical range of outcrop, steep cliffs and
205 rainforest-covered flanks limit the area that can be sampled. However, previous
206 work has shown the remarkable lateral homogeneity of AMS fabrics in plutons at
207 a range of scales, with variations in fabric orientations occurring around a mean
208 vector (Bouchez, 1997; Olivier et al., 1997). What is less constrained is the degree
209 AMS fabric heterogeneity vertically through a pluton. The 2900m vertical range of
210 outcrop at Mt Kinabalu provides a unique opportunity to explore this, and
211 consequently sampling focussed on transects to the North, South, East and West
212 of the pluton. Samples were collected at 50m vertical intervals on the summit and
213 the accessible southern flank, and at 100m vertical intervals elsewhere.

214 94 oriented block samples were collected (Fig. 5) from which 10 to 24 cylindrical
215 cores of 11cm³ were drilled per sample at the University of Birmingham, UK
216 (Owens, 1994) The number of cores depended on each sample's weathering and
217 alteration. Oriented cores were analysed on an AGICO KLY-3s Kappabridge at the
218 University of Birmingham to determine the orientation and magnitude (K) of the
219 three principal axes of the AMS fabric (K_1 , K_2 and K_3 ; Fig. 1). Each sub-specimen's
220 results were normalised by the specimen's mean susceptibility (K_{mean}) and
221 averaged for each block sample to determine mean values of the AMS ellipsoid
222 (Jelínek, 1978, Owens, 2000). To determine the magnetic mineralogy, variability
223 of magnetic susceptibility with temperature was determined on powdered
224 samples at the University of Cambridge, UK. An AGICO MFK1 Kappabridge with a
225 CS4 high temperature attachment and CS-L low temperature attachment was used
226 under an argon atmosphere to reduce secondary oxidation. Samples representing
227 each plutonic unit were selected for detailed magnetic characterisation.
228 Hysteresis loops, DC demagnetisation curves and first-order reversal curve
229 (FORC) diagrams were collected using a Lakeshore Vibrating Sample
230 Magnetometer at the University of Cambridge.

231 **6. Results**

232 **6.1. Shape of the AMS fabric**

233 Full results are given in the supplementary material. The shape of the observed
234 AMS fabric is described according to the relative dimensions of the three principal
235 axes of the AMS ellipsoid (Fig. 1). All analysed fabrics lie along a spectrum from
236 purely oblate (a flattened spheroid where $K1 = K2 > K3$) to purely prolate (an
237 elongated spheroid where $K1 > K2 = K3$) and are described by the shape
238 parameter, T (Jelinek, 1981) which has a possible range from 1 (purely oblate) to
239 -1 (purely prolate). The degree of measured anisotropy (P' , Jelinek, 1981) is used
240 instead of $K1/K3$ as it refers to deviation of all axes (including $K2$) from the mean
241 susceptibility. The bulk magnetic susceptibility (K_{Mean}) varies by two orders of
242 magnitude (Fig. 6). The mineral fabric (T) is dominantly oblate (Fig. 6), but for
243 almost all samples the axes are statistically distinct from each other at 95%
244 confidence; allowing statistically valid utilisation of all three axes (including the
245 lineation, $K1$).

246 **6.2. Magnetic mineralogy**

247 The magnetically susceptible mineralogy can be determined from the variations
248 of magnetic susceptibility with temperature (Fig. 7), hysteresis loops (Fig. 8) and
249 First Order Reversal Curves (FORC diagrams, Fig. 8). All samples except the
250 Alexandra Tonalite/Granodiorite show abrupt reductions in bulk susceptibility on
251 heating between 565-585°C, the Curie temperature of pure magnetite. Although a
252 small Hopkinson peak prior to the 565-585°C reduction in magnetic susceptibility
253 appears to be present in some samples (Fig. 7), the lack of an extreme peak
254 indicates dominance of multi-domain rather than single or pseudo single-domain
255 particles (Orlický, 1990). The susceptibility decrease at 320-420°C results from
256 the conversion of maghemitised magnetite to hematite (Orlický, 1990), an
257 interpretation supported by the absence of this feature in the cooling curves. For
258 all samples the cooling curve has a higher susceptibility than the heating curve,
259 indicating production of secondary magnetite during heating.

260 The low bulk susceptibility of the Alexandra Tonalite/Granodiorite indicates a
261 paramagnetic carrier phase, most probably biotite and/or amphibole, given the

262 mineralogy of this unit (Burton-Johnson et al., 2017). This is consistent with the
263 parabolic decrease in susceptibility at low temperature (Fig. 7) with no increase at
264 -148°C (the Verwey transition; Walz 2002), indicating that magnetite is not the
265 dominant carrier. The hysteresis loops have a high contribution from
266 paramagnetic minerals, which were corrected for in the analysis (Fig. 8). The
267 samples have low coercivity values in the range of 2.7-8.5 mT, consistent for multi-
268 domain grains (see supplementary material for full results). FORC diagrams for
269 the Alexandra Tonalite/Granodiorite and King Granite (Fig. 8) show low coercivity
270 (B_c) and a wide range in the bias field (B_u), with a weakly expressed negative bias
271 region present on the right hand side of the lobe. These features all indicate multi-
272 domain behaviour, as even small proportions of single-domain grains produce the
273 high coercivity and narrow bias range associated with single-domain behaviour
274 (Fig. 8; Harrison et al., 2018). As the magnetic fabric is and hosted by multi-domain
275 magnetite, biotite, and amphibole, the AMS data does not represent an inverse
276 fabric (as would be produced by single-domain magnetite; Stephenson et al.,
277 1986).

278 **6.3. AMS fabric of the different units**

279 Overall the fabrics of most Mt Kinabalu granitic units display lineation with a
280 shallow, NW plunge (K1; Fig. 9), and shallow dipping foliation (to which K3 is the
281 pole; Fig. 8), although there are deviations. In the Alexandra
282 Tonalite/Granodiorite, lineation of the AMS fabric (K1) shows a shallow plunge to
283 the NW whilst the foliation (K3) has a consistent moderate dip to the SW (Fig. 9).
284 Lineation of the Low's Granite also plunges to the NW but the foliation dip is
285 shallower than the Alexandra unit (Fig. 9). The most sampled unit, the King
286 Granite, has the most homogenous AMS fabric with a lineation consistently
287 plunging sub-horizontally to the NW/SE and a foliation recording a very shallow
288 SW dip (Fig. 9). The Donkey Granite has the lowest areal extent and thus the
289 fewest samples. Its lineation is variable and dominantly contact-parallel (Fig. 9)
290 while the foliation has a shallow west dip (Fig. 9), although it frequently strikes
291 sub-parallel to the contacts (Fig. 5). The AMS fabric of the Paka Porphyritic Granite
292 again has a shallow NW plunge to its lineation and a shallow west dip to its
293 foliation (Fig. 9). However, deviations in both the lineation and foliation are

294 evident at the eastern extent and near internal contacts (Fig. 5). We obtained
295 relatively few measurements of the Mesilau Porphyritic Granite due to the poor
296 accessibility of the lower forested flanks of Mt Kinabalu. AMS measurements of
297 Mesilau are highly variable in both foliation and lineation (Fig. 9). Thin section
298 examinations of this unit reveal accumulations of secondary hydrothermal
299 magnetite within its fractures and along grain boundaries, leading to the poorly
300 defined AMS fabric (Fig. 9) and largest range of bulk susceptibility (Fig. 6).

301 **7. Discussion**

302 **7.1. Tectonic or magmatic fabric?**

303 The AMS fabric of Mt Kinabalu shows clear and consistent orientations through
304 most units but to understand the origin of this fabric we must determine if it
305 represents magmatic or tectonic strain. This distinction is achieved by comparing
306 the AMS fabric with field evidence for tectonic strain (Paterson et al., 1998).
307 Burton-Johnson et al. (2017) investigated the orientations and relationship of
308 several, early, post-magmatic strain indicators in and around Mt. Kinabalu,
309 including orientations of faults, aplite dykes and mafic dykes within the pluton.
310 These indicate a post-magmatic sub-vertical principal compressive stress, σ_1 (i.e.
311 lithostatic pressure), whilst the minimum compressive stress, σ_3 , was sub-
312 horizontally NNW-SSE oriented (Fig. 10). This extensional regime contrasts with
313 the NW-SE to N-S striking compressive folds and associated thrust faults of the
314 local sedimentary country rocks (Jacobson, 1970; Burton-Johnson et al., 2017),
315 which record the Early Miocene Sabah Orogeny (Hutchison, 1996) that pre-dates
316 the intrusion.

317 Under coaxial shear, the extensional stress field recorded by the faults and dykes
318 of the pluton (Fig. 10) would be predicted to generate AMS fabrics with shallow
319 NNW-SSE plunging lineations (K1) and sub-vertically dipping poles to the
320 foliations (K3); similar to Fig. 2c. Fig. 10 shows that this is precisely the syn-
321 magmatic AMS fabric demonstrated by all units except the Donkey Granite and the
322 Mesilau Porphyritic Granite (a result of secondary magnetite), indicating similar
323 syn- and post-magmatic stress regimes. The similarity in the predicted directions
324 of extension from both the field and AMS evidence requires agreement between

325 the principal stress and strain vectors, indicating the dominance of coaxial, non-
326 rotational shear rather than non-coaxial simple shear in the development of the
327 AMS fabric (Fig. 2).

328 As discussed above, the crystallisation of secondary magnetite in the Mesilau
329 Porphyritic Granite has compromised its magnetic record. The foliation of the
330 Donkey Granite shows shallow dips (Fig. 9), however its lineations tend towards
331 contact-parallel orientations rather than the expected fabric. This orientation of
332 contact-parallel lineation and shallow foliation is generated in dykes through
333 post-flow compaction of a contact-parallel magmatic fabric (Park et al., 1988;
334 Ernst and Baragar, 1992), indicating that the deviation of the Donkey Granite
335 fabric from the overall distribution results from the narrow width of this unit
336 (Burton-Johnson et al., 2017).

337 **7.2. Effect of contacts on tectonic AMS fabrics**

338 The mechanical contrast along internal or external contacts will generate contact-
339 parallel fabrics in plutons. Simple shear elongation of the fabric will occur in the
340 stretching direction (Fig. 2d, Paterson and Tobisch, 1988; Paterson et al., 1998).
341 We have noted this effect in the narrow Donkey Granite but how far from a contact
342 does this affect AMS fabric in the larger units?

343 The contact between the King Granite and the later Paka Porphyritic Granite can
344 be traced for over 2km on the south flank of Mt Kinabalu (Fig. 5). Samples from
345 either side of the contact show that the lineation in both units reflects the tectonic
346 overprint even from samples <5m from the contact (Fig. 5c). The foliation is more
347 sensitive to contact-parallel fabrics, with the strike of samples close to the
348 boundary rotated towards the contact but only for samples up to 100m from the
349 contact (Fig. 5d). The presence of a contact-parallel foliation but a tectonic fabric in
350 the lineation indicates rotation about a lineation-parallel zone axis or the
351 development of a variably contact-parallel fabric, subsequently overprinted by
352 invariable extension in the lineation direction.

353 As observed in studies of other intrusions (Bouchez, 1997; Olivier et al., 1997), the
354 AMS fabric of Mt Kinabalu shows remarkable lateral homogeneity across the
355 pluton. The vertical range of exposure at Mt Kinabalu also reveals comparable

356 vertical homogeneity. Overprinting of magmatic fabrics by tectonic strain from
357 coaxial, non-rotational shear is pervasive, even <5m from the contacts and across
358 the entire 2900m vertical range of the intrusion. This implies that plutonic AMS
359 fabrics can be used to determine syn-magmatic tectonic strain even when the
360 geometry of the pluton is unknown.

361 **7.3. Application of the AMS fabric to tectonic interpretation**

362 Excluding the two units for which the tectonic fabric is not recorded (The Donkey
363 Granite and Mesilau Porphyritic Granite), the orientations of the maximum (σ_1)
364 and minimum (σ_3) syn-magmatic tectonic compression directions interpreted
365 from AMS are in close agreement with the field evidence (Fig. 10). However, unlike
366 the syn-magmatic strain recorded by the AMS fabric, because faults and dykes
367 must postdate their host they can only date post-magmatic deformation. The AMS
368 data is also less dispersed, and less ambiguous as its vectors correspond with
369 specific vectors of the strain ellipsoid. As the AMS fabric is hosted by the rock itself,
370 it can be dated directly (unlike most faults and other evidence for paleostrain)
371 allowing determination of the strain ellipsoid at a specific time. This provides a
372 powerful tool for structural and tectonic research.

373 The paleomagnetic rotation of the Mt Kinabalu intrusions since emplacement was
374 determined from granitic samples as 11° anticlockwise ($\pm 2.4^\circ$ at 95% confidence,
375 (Fuller et al., 1991). By correcting the azimuth of the lineation (eigenvector of 308°
376 $\pm 10.7^\circ$ at 95% confidence, the proxy for the syn-magmatic extension direction) by
377 the paleomagnetic rotation we can determine that at 7.9-7.3 Ma Sabah was
378 undergoing NW-SE crustal extension at $319^\circ \pm 13.1^\circ$. This supports the presence
379 of a NW-SE oriented extensional regime in Sabah during the Miocene, which may
380 be the result of SE-directed slab rollback during subduction of the Celebes Sea to
381 the SE (Cottam et al., 2013; Hall, 2013). Our findings are not compatible with
382 models invoking contemporaneous tectonic compression in the region
383 (Hutchison, 2000; Swauger et al., 2000; King et al., 2010; Pubellier and Morley,
384 2013). Emplacement during regional extension is more consistent with a setting
385 affected by slab rollback, which has been proposed between 11-10 Ma (Hall,
386 2013), although our observations suggest that extension persistent until, at least,
387 7.5Ma..

388 **7.4. Tectonic overprinting of magmatic AMS fabrics: A widespread**
389 **phenomenon?**

390 We have shown that extensional tectonics pervasively overprinted the AMS fabric
391 of the Mt Kinabalu intrusion. Where observed elsewhere, similar observations
392 have been utilised to infer local strain partitioning (Archanjo et al., 1992, 2002;
393 Benn, 2010), but can AMS be applied to determine tectonic deformation on a
394 global scale? To investigate whether similar overprinting occurs elsewhere we
395 compiled data from intrusions of varying age and dimensions, and from globally
396 distributed compressional and extensional tectonic regimes (Fig. 11). Whilst not
397 a complete global dataset, this provides a global distribution of plutons from
398 known tectonic settings for which there is comprehensive sample coverage, and
399 includes numerous well-recognised studies (e.g. Mt Stuart, Monte Capanne,
400 Dinkey Creek, and Mono Creek – respectively (Bouillin et al., 1993; de Saint
401 Blanquat and Tikoff, 1997; Cruden, 1999; Benn et al., 2001).. The tectonic settings
402 and orientations of compression or extension are from the literature, with the
403 specific orientation shown in Fig. 11 determined by ourselves as in Fig. 1.

404 Some of the AMS datasets included in our compilation have already been
405 interpreted as recording a tectonic overprint (e.g. the Shellenbarger and Mt Stuart
406 plutons, USA) whilst others have not (e.g. the Pinto Peak intrusion, USA, and the
407 Monte Capanne intrusion, Italy). However, in all cases a clear and consistent fabric
408 is shown by each intrusion. For each example included in our study the orientation
409 of tectonic strain required to generate each fabric through coaxial shear (as
410 illustrated in Fig. 2) is always in agreement with the contemporaneous tectonic
411 regime of the region (Fig. 11).

412 As with Mt Kinabalu, the close agreement of the AMS fabric vectors and regional
413 tectonic stress directions in both compressional and extensional settings indicates
414 the dominance of coaxial, non-rotational shear rather than simple, non-coaxial
415 shear in pluton-scale AMS fabrics. This allows simple interpretation of the stress
416 and strain vectors. Even in plutons associated with major shear zones, field studies
417 have shown that simple shear is only pervasive close to the shear zone (Gleizes et
418 al., 2001; Tikoff et al., 2005; Benn, 2010), returning to more homogenous, coaxial,
419 non-rotational shear fabrics at greater distances from the shear zone; as observed

420 near the contacts of Mt Kinabalu. The pervasiveness of the simple shear regime is
421 dependent on the rheology of the lithology, timing and degree of shearing, and the
422 scale-dependant cooling history of the pluton (Archanjo et al., 2002; Tikoff et al.,
423 2005; Benn, 2010). Where intrusions were metamorphosed and recrystallised in
424 the deeper crust after emplacement, this coaxial tectonic fabric can be imparted
425 millions of years after magmatism (Hrouda et al., 1988; Hrouda and Faryad, 2017).

426 In extensional plutons the lineation direction (K1) is consistently parallel to the
427 azimuth of extension, whilst the foliation dip varies, similar to our observations in
428 the Alexandra Tonalite/Granodiorite of Mt Kinabalu. Similarly, in compressional
429 plutons the pole to foliation (K3) is consistently in the direction of compression
430 whilst the plunge of the lineation varies. In a compressive regime this lineation
431 variation reflects whether σ_2 (Fig. 1) represents lithostatic (vertical) or lateral
432 (tectonic) compression. If σ_2 represents lithostatic compression the lineation will
433 be sub-horizontal but if the degree of tectonic compression is increased and σ_2
434 becomes horizontal then the lineation will be sub-vertical (Fig. 2a and 2b).
435 Similarly, in an extensional regime the foliation variation reflects the orientation
436 of σ_1 (Fig. 1). If σ_1 represents lithostatic compression the foliation will be sub-
437 horizontal but if the degree of lateral compression increases, and σ_1 becomes
438 horizontal then the foliation dip will be sub-vertical.

439 Because of these variations in extensional foliation and compressional lineation,
440 comparing the confidence limits of the mean K1 and K3 vectors (Fig. 12)
441 distinguishes whether a pluton was emplaced in a compressive or extensional
442 setting even in the absence of other data (e.g. field evidence for deformation).
443 Using symmetrical 95% confidence angles for the mean spherical vectors of K1
444 and K3, compressional plutons can be identified at 90% confidence where “K1
445 confidence angle / K3 confidence angle” <1.2, and extensional plutons can be
446 identified at 90% confidence where “K1 confidence angle / K3 confidence angle”
447 >1.5 (Fig. 12).

448 We conclude that coaxial tectonic strain is commonly preserved in the AMS fabric
449 of plutonic intrusions. This explains the remarkable homogeneity of AMS fabrics
450 within many individual plutons (Bouchez, 1997; Olivier et al., 1997) and opens up
451 the possibility of using AMS fabrics to determine syn-magmatic deformation. As

452 intrusive magmatism is a common feature of many tectonic settings throughout
453 Earth's history, the nature of a tectonic regime can be investigated from its
454 accompanying plutons. Just like traditional structural evidence, granitic
455 magmatism has long been seen as a product of tectonic deformation (Vigneresse,
456 1999). By applying this technique, plutons can be used as a potent structural tool
457 for investigating those tectonic processes and identifying tectonic regimes.

458 **8. Conclusions**

459 - The AMS fabric of the Mt Kinabalu intrusion, Borneo, was largely derived by syn-
460 magmatic crustal extension.

461 - Tectonic strain is highly pervasive throughout the Mt Kinabalu pluton,
462 dominating the AMS foliation to within 100m of contact surfaces, and the AMS
463 lineation to <5m from contact surfaces.

464 - After paleomagnetic correction for rotation, the AMS data indicates that crustal
465 extension in Sabah at 7.9-7.3 Ma was oriented NW-SE at $319^\circ \pm 13.1^\circ$. This is
466 consistent with other evidence for Late Miocene extension in NW Borneo (Hall,
467 2013).

468 - In compressive settings, AMS foliations are consistent but lineations vary.
469 Likewise, in extensional settings, AMS lineations are consistent but foliations vary.
470 Consequently, compressional plutons can be distinguished by the relative scales
471 of the K1 and K3 confidence angles.

472 - A compilation of global AMS data for intrusions in extensional and compressional
473 regimes reveals the common occurrence of magnetic fabrics preserving tectonic
474 strain. This indicates that the AMS fabrics of plutonic rocks have the potential to
475 be employed globally to determine syn-magmatic tectonic settings.

476

477 **9. Acknowledgements**

478 This study was funded by the Natural Environment Research Council. We thank
479 Carl Stevenson at the University of Birmingham for providing equipment and
480 training for our AMS analyses and discussion of our results. We wish to thank
481 Robert Hall, Mike Cottam and the SE Asia Research Group at Royal Holloway for
482 their support and discussions throughout this project. We thank Alim Biun, Felix
483 Tongkul and Maklarin Lakim for their assistance in facilitating the field season;
484 Jamili Nais of Sabah Parks who allowed us to work in the National Park; and the
485 mountain guides and researchers of Mt Kinabalu National Park, especially Alijen
486 “Jen”, Halli, Jasirin, Sokaibin, Maklarin Lakim, Sapinus, Samuel and Nicholas. We
487 thank Ian Alsop for his work as Editor in reviewing this paper, and an Anonymous
488 reviewer and František Hrouda and for taking the time to review our submission.
489 To receive such a positive review is greatly encouraging.

490 **10. References**

491

492 Aranguren, a., Cuevas, J., TubIa, J.M., RomAn-Berdiel, T., Casas-Sainz, A., Casas-
493 Ponsati, A., 2003. Granite laccolith emplacement in the Iberian arc: AMS and
494 gravity study of the La Tojiza pluton (NW Spain). *Journal of the Geological*
495 *Society* 160, 435–445. <https://doi.org/10.1144/0016-764902-079>

496 Arbaret, L., Diot, H., Bouchez, J.L., Lespinasse, P., de Saint-Blanquat, M., 1997.
497 Analogue 3D simple-shear experiments of magmatic biotite subfabrics. *Granite:*
498 *From Segregation of Melt to Emplacement Fabrics*. Springer, 129–143.

499 Arbaret, L., Fernandez, A., Ježek, J., Ildefonse, B., Launeau, P., Diot, H., 2000.
500 Analogue and numerical modelling of shape fabrics: application to strain and
501 flow determination in magmas. *Geological Society of America Special Papers*
502 350, 97–109.

503 Archanjo, C.J., da Silva, E.R., Caby, R., 1999. Magnetic fabric and pluton emplacement
504 in a transpressive shear zone system: the Itaporanga porphyritic granitic pluton
505 (northeast Brazil). *Tectonophysics* 312, 331–345.

506 Archanjo, C.J., Olivier, P., Bouchez, J.L., 1992. Plutons granitiques du Seridó (NE du
507 Brésil): écoulement magmatique parallèle à la chaîne révélé par leur anisotropie
508 magnétique. *Bull. Sac. Géol. France* 163, 509–520.

509 Archanjo, C.J., Trindade, R.I., Bouchez, J.L., Ernesto, M., 2002. Granite fabrics and
510 regional-scale strain partitioning in the Seridó belt (Borborema Province, NE
511 Brazil). *Tectonics* 21, 1003.

512 Benn, K., 2010. Anisotropy of magnetic susceptibility fabrics in syntectonic plutons as
513 tectonic strain markers: the example of the Canso pluton, Meguma Terrane,
514 Nova Scotia. *Earth and Environmental Science Transactions of the Royal*
515 *Society of Edinburgh* 100, 147–158.
516 <https://doi.org/10.1017/S1755691009016028>

517 Benn, K., Paterson, S.R., Lund, S.P., Pignotta, G.S., Kruse, S., 2001. Magmatic fabrics
518 in batholiths as markers of regional strains and plate kinematics: example of the
519 Cretaceous Mt. Stuart batholith. *Physics and Chemistry of the Earth, Part A:*
520 *Solid Earth and Geodesy* 26, 343–354. [https://doi.org/10.1016/S1464-](https://doi.org/10.1016/S1464-1895(01)00064-3)
521 [1895\(01\)00064-3](https://doi.org/10.1016/S1464-1895(01)00064-3)

522 Blumenfeld, P., Bouchez, J.-L., 1988. Shear criteria in granite and migmatite deformed
523 in the magmatic and solid states. *Journal of Structural Geology* 10, 361–372.
524 [https://doi.org/10.1016/0191-8141\(88\)90014-4](https://doi.org/10.1016/0191-8141(88)90014-4)

525 Bouchez, J.L., 1997. Granite is never isotropic: an introduction to AMS studies of
526 granitic rocks. *Granite: From Segregation of Melt to Emplacement Fabrics*.
527 Springer, 95–112.

528 Bouillin, J.-P., Bouchez, J.-L., Lespinasse, P., Pe^cher, a., 1993. Granite emplacement
529 in an extensional setting: an AMS study of the magmatic structures of Monte
530 Capanne (Elba, Italy). *Earth and Planetary Science Letters* 118, 263–279.
531 [https://doi.org/10.1016/0012-821X\(93\)90172-6](https://doi.org/10.1016/0012-821X(93)90172-6)

532 Bucher, K., Grapes, R., 2011. *Petrogenesis of metamorphic rocks*, 8th Edition. ed.
533 Springer, Heidelberg, Germany.

534 Burton-Johnson, A., Macpherson, C.G., Hall, R., 2017. Internal structure and
535 emplacement mechanism of composite plutons: evidence from Mt Kinabalu,
536 Borneo. *Journal of the Geological Society* 174, 180–191.

537 Burton-Johnson, A., Macpherson, C.G., Ottley, C.J., Nowell, G.M., Boyce, A.J., in
538 review. Generation of Mt Kinabalu granite by crustal contamination of

539 intraplate magma modelled by Equilibrated Major Element Assimilation with
540 Fractional Crystallisation (EME-AFC). *Journal of Petrology*.

541 Collenette, P., 1965. The geology and mineral resources of the Pensiangan and Upper
542 Kinabatangan area, Sabah. Malaysia Geological Survey Borneo Region,
543 Memoir 12 150.

544 Cottam, M.A., Hall, R., Sperber, C., Armstrong, R., 2010. Pulsed emplacement of the
545 Mount Kinabalu granite, northern Borneo. *Journal of the Geological Society*
546 167, 49–60. <https://doi.org/10.1144/0016-76492009-028>. Pulsed

547 Cottam, M.A., Hall, R., Sperber, C., Kohn, B.P., Forster, M.A., Batt, G.E., 2013.
548 Neogene rock uplift and erosion in northern Borneo: evidence from the
549 Kinabalu granite, Mount Kinabalu. *Journal of the Geological Society* 170, 805–
550 816. <https://doi.org/10.1144/jgs2011-130>

551 Cruden, A.R., 1999. Magnetic fabric evidence for conduit-fed emplacement of a tabular
552 intrusion: Dinkey Creek Pluton, central Sierra Nevada batholith, California.
553 *Journal of Geophysical Research: Solid Earth* 104, 511–530.

554 Davis, J.C., 1986. *Statistics and data analysis in geology*, 2nd Edition. ed. Wiley &
555 Sons, New York.

556 de Saint Blanquat, M., Tikoff, B., 1997. Development of magmatic to solid-state fabrics
557 during syntectonic emplacement of the Mono Creek Granite, Sierra Nevada
558 Batholith. *Granite: From Segregation of Melt to Emplacement Fabrics*.
559 Springer, 231–252.

560 Deng, X., Wu, K., Yang, K., 2013. Emplacement and deformation of Shigujuan
561 syntectonic granite in central part of the Dabie orogen: Implications for tectonic
562 regime transformation. *Science China Earth Sciences* 56, 980–992.

563 Dhonau, T.J., Hutchison, C.S., 1965. The Darvel Bay area, East Sabah, Malaysia.
564 Malaysia Geological Survey Borneo Region, Annual Report for 1965 141–160.

565 Ernst, R.E., Baragar, W.R.A., 1992. Evidence from magnetic fabric for the flow pattern
566 of magma in the Mackenzie giant radiating dyke swarm. *Nature* 356, 511.

567 Fuller, M., Haston, R., Lin, J., Richter, B., 1991. Tertiary paleomagnetism of regions
568 around the South China Sea. *Journal of Southeast ...* 6, 161–184.

569 Gay, N. C., 1968. The motion of rigid particles embedded in a viscous fluid during pure
570 shear deformation of the fluid. *Tectonophysics* 5, 81–88.

571 Gay, No C., 1968. Pure shear and simple shear deformation of inhomogeneous viscous
572 fluids. 1. Theory. *Tectonophysics* 5, 211–234.

573 Gleizes, G., Leblanc, D., Olivier, P., Bouchez, J., 2001. Strain partitioning in a pluton
574 during emplacement in transpressional regime: the example of the Néouvielle
575 granite (Pyrenees). *International Journal of Earth Sciences* 90, 325–340.

576 Grove, C., Jerram, D.A., 2011. jPOR: An ImageJ macro to quantify total optical
577 porosity from blue-stained thin sections. *Computers & Geosciences* 37, 1850–
578 1859.

579 Gutiérrez, F., Payacán, I., Gelman, S.E., Bachmann, O., Parada, M. a., 2013. Late-stage
580 magma flow in a shallow felsic reservoir: Merging the anisotropy of magnetic
581 susceptibility record with numerical simulations in La Gloria Pluton, central
582 Chile. *Journal of Geophysical Research: Solid Earth* 118, 1984–1998.
583 <https://doi.org/10.1002/jgrb.50164>

584 Hall, R., 2013. Contraction and extension in northern Borneo driven by subduction
585 rollback. *Journal of Asian Earth Sciences* 76, 399–411.
586 <https://doi.org/10.1016/j.jseaes.2013.04.010>

587 Harrison, R.J., Muraszko, J., Heslop, D., Lascu, I., Muxworthy, A.R., Roberts, A.P.,
588 2018. An Improved Algorithm For Unmixing First-Order Reversal Curve

589 Diagrams Using Principal Component Analysis. *Geochemistry, Geophysics,*
590 *Geosystems.*

591 Hrouda, F., Faryad, S.W., 2017. Magnetic fabric overprints in multi-deformed
592 polymetamorphic rocks of the Gemic Unit (Western Carpathians) and its
593 tectonic implications. *Tectonophysics* 717, 83–98.

594 Hrouda, F., Jacko, S., Hanák, J., 1988. Parallel magnetic fabrics in metamorphic,
595 granitoid and sedimentary rocks of the Branisko and Čierna Hora Mountains (E
596 Slovakia) and their tectonometamorphic control. *Physics of the Earth and*
597 *Planetary Interiors* 51, 271–289.

598 Hrouda, F., Ježek, J., 2017. Role of single-domain magnetic particles in creation of
599 inverse magnetic fabrics in volcanic rocks: A mathematical model study. *Studia*
600 *Geophysica et Geodaetica* 61, 145–161.

601 Hunt, C.P., Moskowitz, B.M., Banerjee, S.K., 1995. Magnetic properties of rocks and
602 minerals. In: Ahrens, T.J. (Ed.), *Rock Physics & Phase Relations: A Handbook*
603 *of Physical Constants.* AGU, Washington D.C., 189–204.

604 Hutchison, C., 2000. A Miocene collisional belt in north Borneo: uplift mechanism and
605 isostatic adjustment quantified by thermochronology. *Journal of the Geological*
606 *Society* 157, 783–793.

607 Hutchison, C.S., 1996. The “Rajang accretionary prism” and “Lupar Line” problem of
608 Borneo. *Geological Society, London, Special Publications* 106, 247–261.
609 <https://doi.org/10.1144/GSL.SP.1996.106.01.16>

610 Hutton, D.H., 1988. Granite emplacement mechanisms and tectonic controls:
611 inferences from deformation studies. *Earth and Environmental Science*
612 *Transactions of the Royal Society of Edinburgh* 79, 245–255.

613 Jacobson, G., 1970. Gunung Kinabalu Area, Sabah, Malaysia. *Geological Survey*
614 *Malaysia, Kuching, Sarawak.*

615 Jeffery, G.B., 1922. The motion of ellipsoidal particles immersed in a viscous fluid.
616 *Proc. R. Soc. Lond. A* 102, 161–179.

617 Ježek, J., Hrouda, F., 2004. Determination of the orientation of magnetic minerals from
618 the anisotropy of magnetic susceptibility. *Geological Society, London, Special*
619 *Publications* 238, 9–20.

620 King, R.C., Backé, G., Morley, C.K., Hillis, R.R., Tingay, M.R.P., 2010. Balancing
621 deformation in NW Borneo: Quantifying plate-scale vs. gravitational tectonics
622 in a delta and deepwater fold-thrust belt system. *Marine and Petroleum Geology*
623 27, 238–246. <https://doi.org/10.1016/j.marpetgeo.2009.07.008>

624 Kirk, H.J.C., 1968. The igneous rocks of Sarawak and Sabah. *Geological Survey*
625 *Borneo Region, Malaysia, Bulletin* 5, 201.

626 Koopmans, B.N., 1967. Deformation of the metamorphic rocks and the Chert–Spilite
627 Formation in the southern part of the Darvel Bay area, Sabah. *Geological*
628 *Survey of Malaysia, Borneo Region, Bulletin* 8, 14–24.

629 Lennox, P.G., de Wall, H., Durney, D.W., 2016. Correlation between magnetic fabrics,
630 strain and biotite microstructure with increasing mylonitisation in the
631 pre-tectonic Wyangala Granite, Australia. *Tectonophysics* 676, 170–197.

632 Leong, K.M., 1974. The geology and mineral resources of the Upper Segama Valley
633 and Darvel Bay area, Sabah, Malaysia. *Geological Survey of Malaysia, Memoir*
634 4.

635 Lin, W., Charles, N., Chen, Y., Chen, K., Faure, M., Wu, L., Wang, F., Li, Q., Wang,
636 J., Wang, Q., 2013. Late Mesozoic compressional to extensional tectonics in the
637 Yiwulüshan massif, NE China and their bearing on the Yinshan–Yanshan

638 orogenic belt: part II: anisotropy of magnetic susceptibility and gravity
639 modeling. *Gondwana Research* 23, 78–94.

640 Martins, H.C., Sant’Ovaia, H., Abreu, J., Oliveira, M., Noronha, F., 2011.
641 Emplacement of the Lavadores granite (NW Portugal): U/Pb and AMS results.
642 *Comptes Rendus Geoscience* 343, 387–396.

643 Olivier, P., de Saint Blanquat, M., Gleizes, G., Leblanc, D., 1997. Homogeneity of
644 granite fabrics at the metre and dekametre scales. *Granite: From Segregation of*
645 *Melt to Emplacement Fabrics*. Springer, 113–127.

646 Orlický, O., 1990. Detection of magnetic carriers in rocks: results of susceptibility
647 changes in powdered rock samples induced by temperature. *Physics of the Earth*
648 *and Planetary Interiors* 63, 66–70.

649 Otoh, S., Jwa, Y.-J., Nomura, R., Sakai, H., 1999. A preliminary AMS (anisotropy of
650 magnetic susceptibility) study of the Namwon granite, southwest Korea.
651 *Geosciences Journal* 3, 31–41.

652 Owens, W.H., 1994. Laboratory drilling of field-orientated block samples. *Journal of*
653 *Structural Geology* 16, 1719–1721. [https://doi.org/10.1016/0191-](https://doi.org/10.1016/0191-8141(94)90137-6)
654 [8141\(94\)90137-6](https://doi.org/10.1016/0191-8141(94)90137-6)

655 Park, J.K., Tanczyk, E.I., Desbarats, A., 1988. Magnetic fabric and its significance in
656 the 1400 Ma Mealy diabase dykes of Labrador, Canada. *Journal of Geophysical*
657 *Research: Solid Earth* 93, 13689–13704.

658 Paterson, S.R., Fowler, T.K., Schmidt, K.L., Yoshinobu, A.S., Yuan, E.S., Miller, R.B.,
659 1998. Interpreting magmatic fabric patterns in plutons. *Lithos* 44, 53–82.
660 [https://doi.org/10.1016/S0024-4937\(98\)00022-X](https://doi.org/10.1016/S0024-4937(98)00022-X)

661 Paterson, S.R., Tobisch, O.T., 1988. Using pluton ages to date regional deformations:
662 problems with commonly used criteria. *Geology* 16, 1108–1111.

663 Petronis, M.S., O’Driscoll, B., 2013. Emplacement of the early Miocene Pinto Peak
664 intrusion, Southwest Utah, USA. *Geochemistry, Geophysics, Geosystems* 14,
665 5128–5145.

666 Petronis, M.S., O’Driscoll, B., Stevenson, C.T.E., Reavy, R.J., 2012. Controls on
667 emplacement of the Caledonian Ross of Mull Granite, NW Scotland:
668 Anisotropy of magnetic susceptibility and magmatic and regional structures.
669 *Geological Society of America Bulletin* 124, 906–927.
670 <https://doi.org/10.1130/B30362.1>

671 Pitcher, W.S., 1997. *The nature and origin of granite*, Second Edition. ed. Chapman &
672 Hall, London, UK.

673 Pubellier, M., Morley, C.K., 2013. The Basins of Sundaland (SE Asia); evolution and
674 boundary conditions. *Marine and Petroleum Geology* 58, 555–578.

675 Reinhard, M., Wenk, E., 1951. *Geology of the Colony of North Borneo*. British Borneo
676 Geological Survey Bulletin 1.

677 Sadeghian, M., Bouchez, J.L., Nédélec, a., Siqueira, R., Valizadeh, M.V., 2005. The
678 granite pluton of Zahedan (SE Iran): a petrological and magnetic fabric study
679 of a syntectonic sill emplaced in a transtensional setting. *Journal of Asian Earth*
680 *Sciences* 25, 301–327. <https://doi.org/10.1016/j.jseas.2004.03.001>

681 Schofield, D.I., D’Lemos, R.S., 1998. Relationships between syn-tectonic granite
682 fabrics and regional PTtd paths: an example from the Gander-Avalon boundary
683 of NE Newfoundland. *Journal of Structural Geology* 20, 459–471.

684 Schulmann, K., Ježek, J., 2012. Some remarks on fabric overprints and constrictional
685 AMS fabrics in igneous rocks. *International Journal of Earth Sciences* 101, 705–
686 714.

687 Schulmann, K., Jezek, J., Venera, Z., 1997. Perpendicular linear fabrics in granite:
688 markers of combined simple shear and pure shear flows? *Granite: From*
689 *Segregation of Melt to Emplacement Fabrics*. Springer, 159–176.

690 Stephenson, A., Sadikun, S. t, Potter, D.K., 1986. A theoretical and experimental
691 comparison of the anisotropies of magnetic susceptibility and remanence in
692 rocks and minerals. *Geophysical Journal International* 84, 185–200.

693 Swauger, D.A., Hutchison, C.S., Bergman, S.C., Graves, J.E., 2000. Age and
694 emplacement of the Mount Kinabalu pluton. *Geological Society of Malaysia*
695 *Bulletin* 44, 159–163.

696 Talbot, J.-Y., Chen, Y., Faure, M., 2005. A magnetic fabric study of the Aigoual–Saint
697 Guiral–Liron granite pluton (French Massif Central) and relationships with its
698 associated dikes. *Journal of Geophysical Research* 110, B12106–B12106.
699 <https://doi.org/10.1029/2005JB003699>

700 Tikoff, B., Davis, M.R., Teyssier, C., Blanquat, M. de S., Habert, G., Morgan, S., 2005.
701 Fabric studies within the Cascade Lake shear zone, Sierra Nevada, California.
702 *Tectonophysics* 400, 209–226.

703 Tomek, F., Žák, J., Verner, K., Holub, F.V., Sláma, J., Paterson, S.R., Memeti, V.,
704 2017. Mineral fabrics in high-level intrusions recording crustal strain and
705 volcano–tectonic interactions: the Shellenbarger pluton, Sierra Nevada,
706 California. *Journal of the Geological Society* 174, 193–208.

707 Tomek, F., Žák, J., Verner, K., Holub, F.V., Sláma, J., Paterson, S.R., Memeti, V.,
708 2016. Mineral fabrics in high-level intrusions recording crustal strain and
709 volcano–tectonic interactions: the Shellenbarger pluton, Sierra Nevada,
710 California. *Journal of the Geological Society* jgs2015-151.
711 <https://doi.org/10.1144/jgs2015-151>

712 van Hattum, M.W., Hall, R., Pickard, A.L., Nichols, G.J., 2006. Southeast Asian
713 sediments not from Asia: Provenance and geochronology of north Borneo
714 sandstones. *Geology* 34, 589–592.

715 Vignerresse, J.-L., 1999. Should felsic magmas be considered as tectonic objects, just
716 like faults or folds? *Journal of Structural Geology* 21, 1125–1130.

717 Vogt, E., Flower, M., 1989. Genesis of the Kinabalu (Sabah) granitoid at a subduction-
718 collision junction. *Contributions to Mineralogy and Petrology* 493–509.

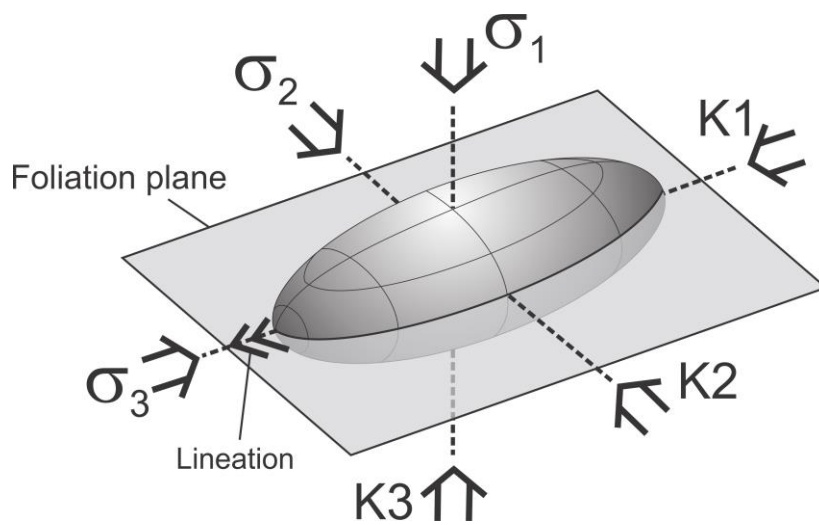
719 Walz, F., 2002. The Verwey transition-a topical review. *Journal of Physics: Condensed*
720 *Matter* 14, R285.

721 Whitney, D.L., Evans, B.W., 2010. Abbreviations for names of rock-forming minerals.
722 *American Mineralogist* 95, 185.

723 Wilson, J., 1998. Magnetic susceptibility patterns in a Cordilleran granitoid: the Las
724 Tazas complex, northern Chile. *Journal of Geophysical Research: Solid Earth*
725 103, 5257–5267.

726

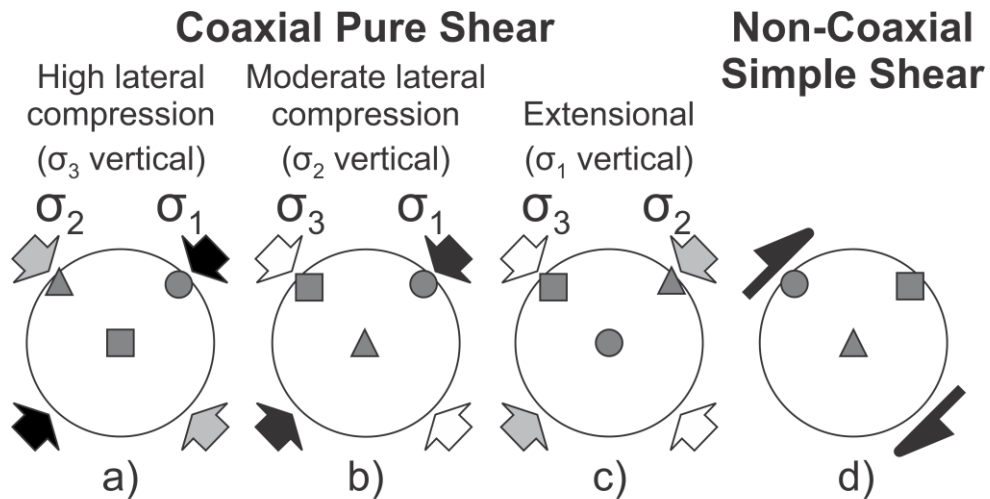
727 **Figures**



728

729 Fig. 1. Relationship of mineral fabrics (foliation and lineation) and the principal
730 vectors of magnetic susceptibility describing the AMS fabric (K1 - Maximum
731 susceptibility; K2 - Intermediate susceptibility; K3 - Minimum susceptibility) to
732 the strain ellipsoid and the principal stress directions during crystallisation (σ_1 -
733 Maximum compression direction; σ_2 . - Intermediate compression direction; σ_3 -
734 Minimum compression direction).

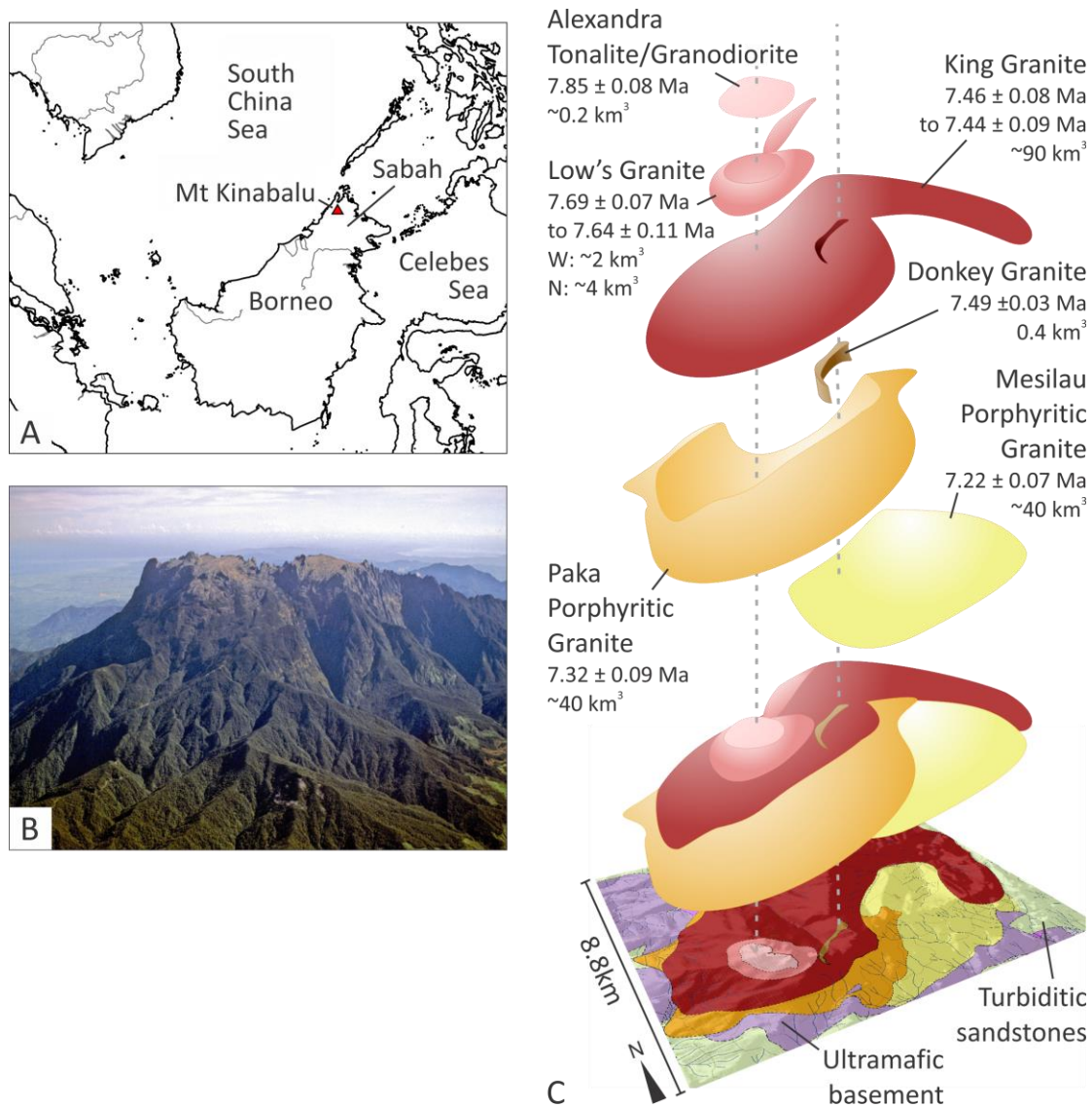
735



736 **AMS Axes:** ■ K1 ▲ K2 ● K3

737 Fig. 2. Example stereonet (lower hemisphere projection) of the resultant AMS
 738 fabrics developed in response to coaxial and non-coaxial strain. Shown are the
 739 principal stress directions, simple shear direction, and principal vectors of
 740 magnetic susceptibility: K1 - Maximum susceptibility; K2 - Intermediate
 741 susceptibility; K3 - Minimum susceptibility.

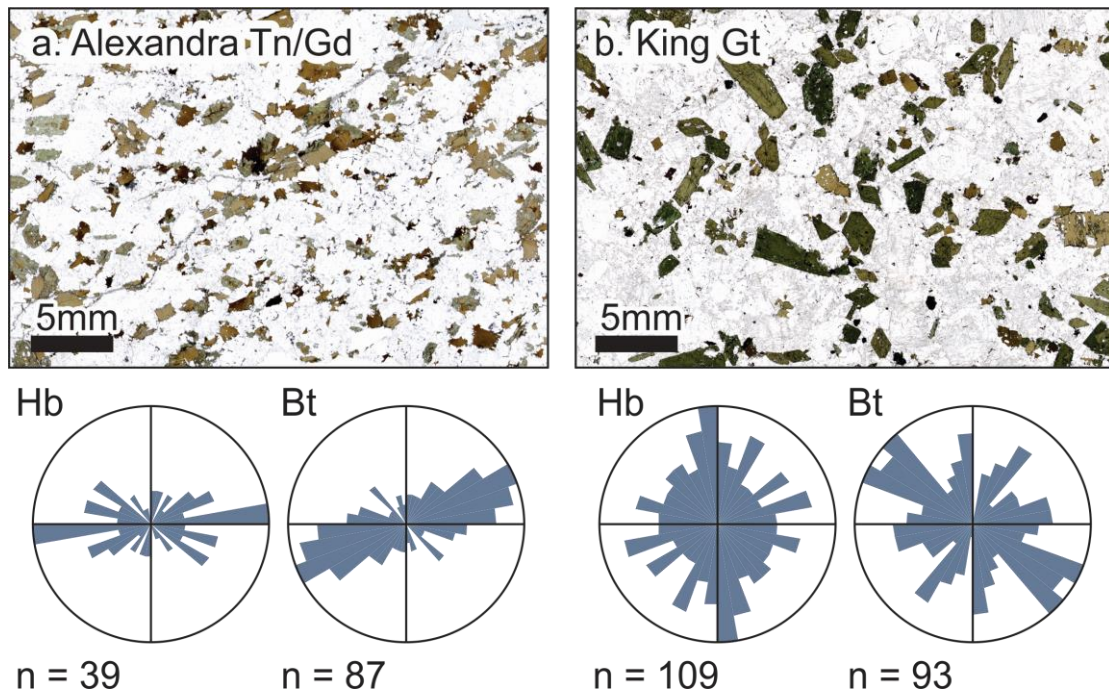
742



743

744 Fig. 3. A) Regional geography of Mt Kinabalu and Sabah within SE Asia. B) Aerial
 745 photograph of Mt Kinabalu from the south highlighting its extreme vertical relief;
 746 courtesy of Tony Barber. C) Internal structure and emplacement ages (Cottam et
 747 al., 2010) of the Mt Kinabalu intrusion, as determined from field evidence (Burton-
 748 Johnson et al., 2017).

749



750

n = 39

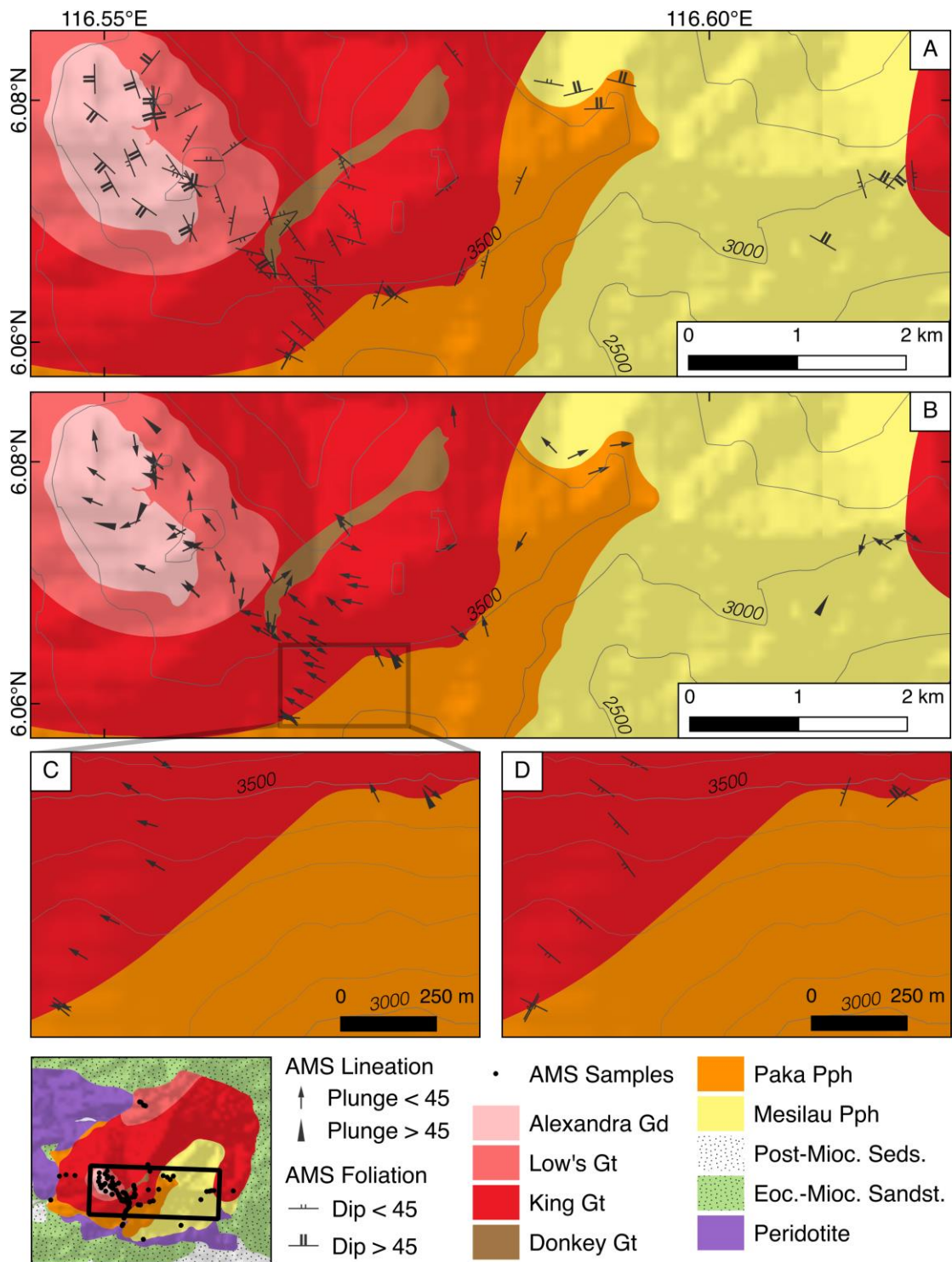
n = 87

n = 109

n = 93

751 Fig. 4. Representative thin section images of (a) the Alexandra
 752 Tonalite/Granodiorite, and (b) the King Granite (itself representative of the post-
 753 Alexandra units). Rose diagrams show the orientations hornblende and biotite
 754 crystals in each section. Sections are arbitrarily orientated. Abbreviations as in Fig.
 755 1, plus Hb – Hornblende; Bt – Biotite.

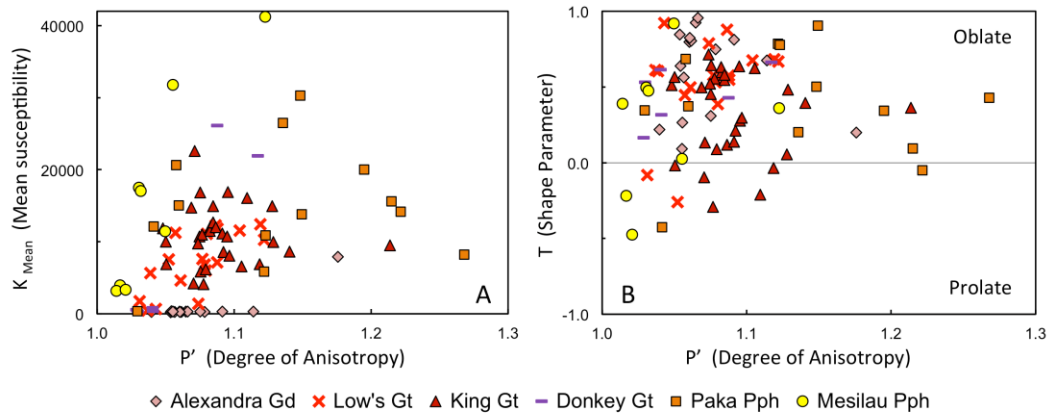
756



757

758 Fig. 5. Geological map of Mt Kinabalu highlighting the (A) foliation and (B)
 759 lineation of the summit plateaux and eastern ridge. Variations in these
 760 orientations close to the contact between the King Granite and Paka Porphyritic
 761 Granite (box shown in B) are shown in (C) and (D). Abbreviations as in Fig. 5.

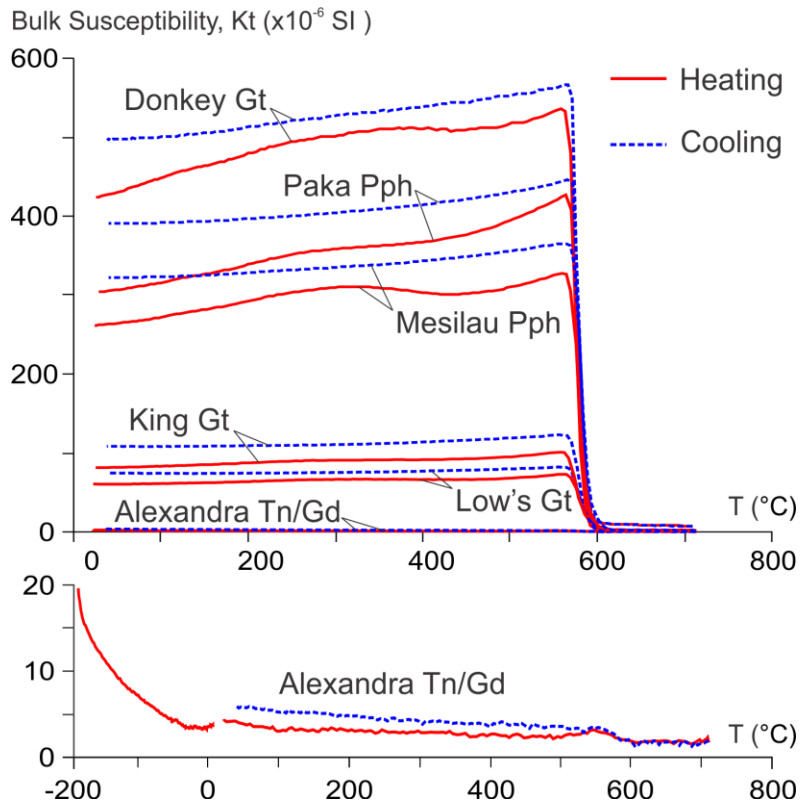
762



763

764 Fig. 6. Relationship of the degree of magnetic anisotropy, P' , to the mean bulk
 765 susceptibility, K_{Mean} (A), and shape parameter of the AMS fabric, T (B).
 766 Abbreviations: Tn – Tonalite, Gd – Granodiorite, Gt – Granite, Pph – Porphyritic
 767 Granite.

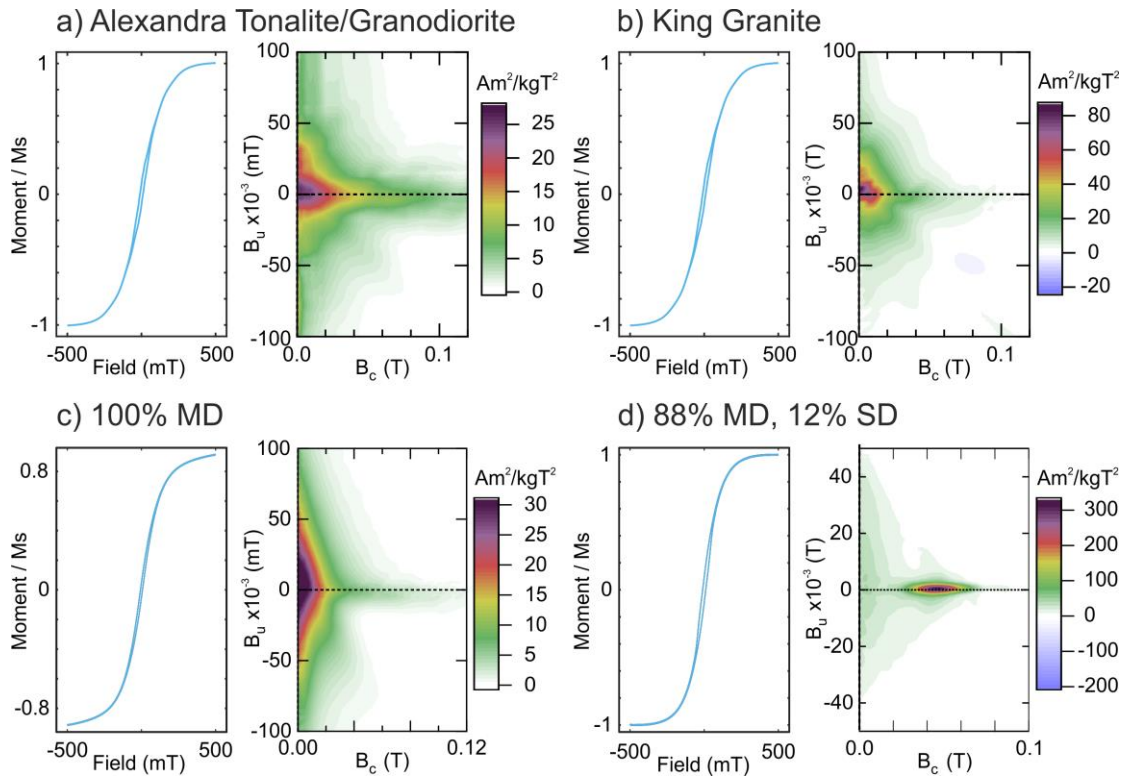
768



769

770 Fig. 7. Variation in bulk magnetic susceptibility of each granitic unit with
 771 temperature. Abbreviations as in Fig. 5.

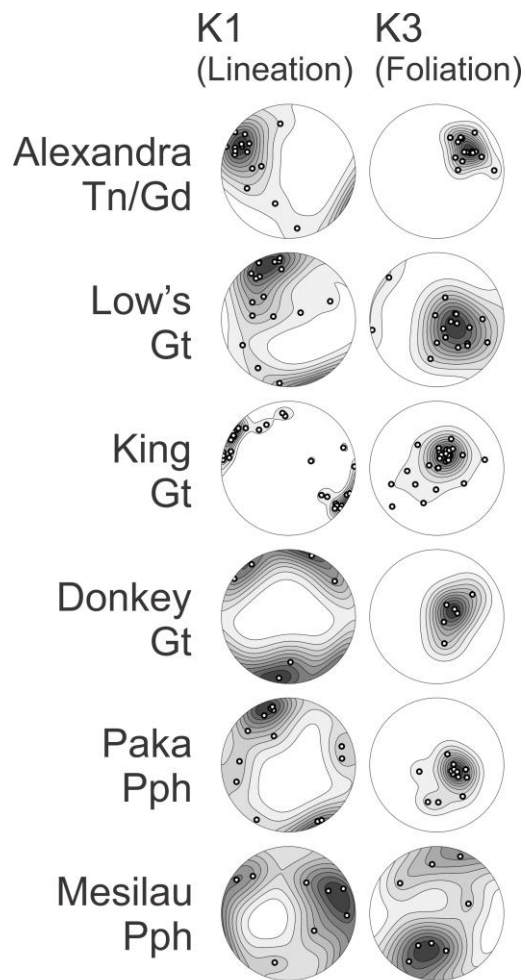
772



773

774 Fig. 8. Hysteresis loops and First Order Reversal curves for: a) the Alexandra
 775 Tonalite/Granodiorite; b) the King Granite. The King Granite is representative of
 776 the plutons' other composite units. Two synthetic binary mixtures of c) purely
 777 multi-domain (MD), and d) a mixture of multi- and single-domain (SD) magnetite
 778 are shown for comparison (Harrison et al., 2018).

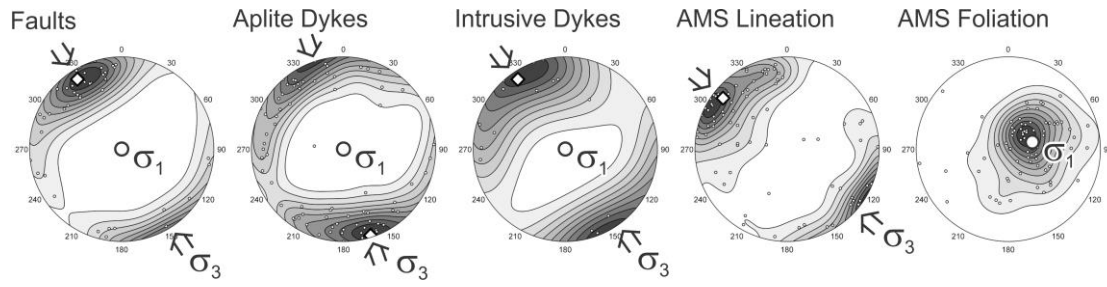
779



780

781 Fig. 9. Lower hemisphere projections of the lineation (K1) and pole to the foliation
 782 (K3) for the AMS fabric of each of Mt Kinabalu's composite units. Abbreviations as
 783 in Fig. 5.

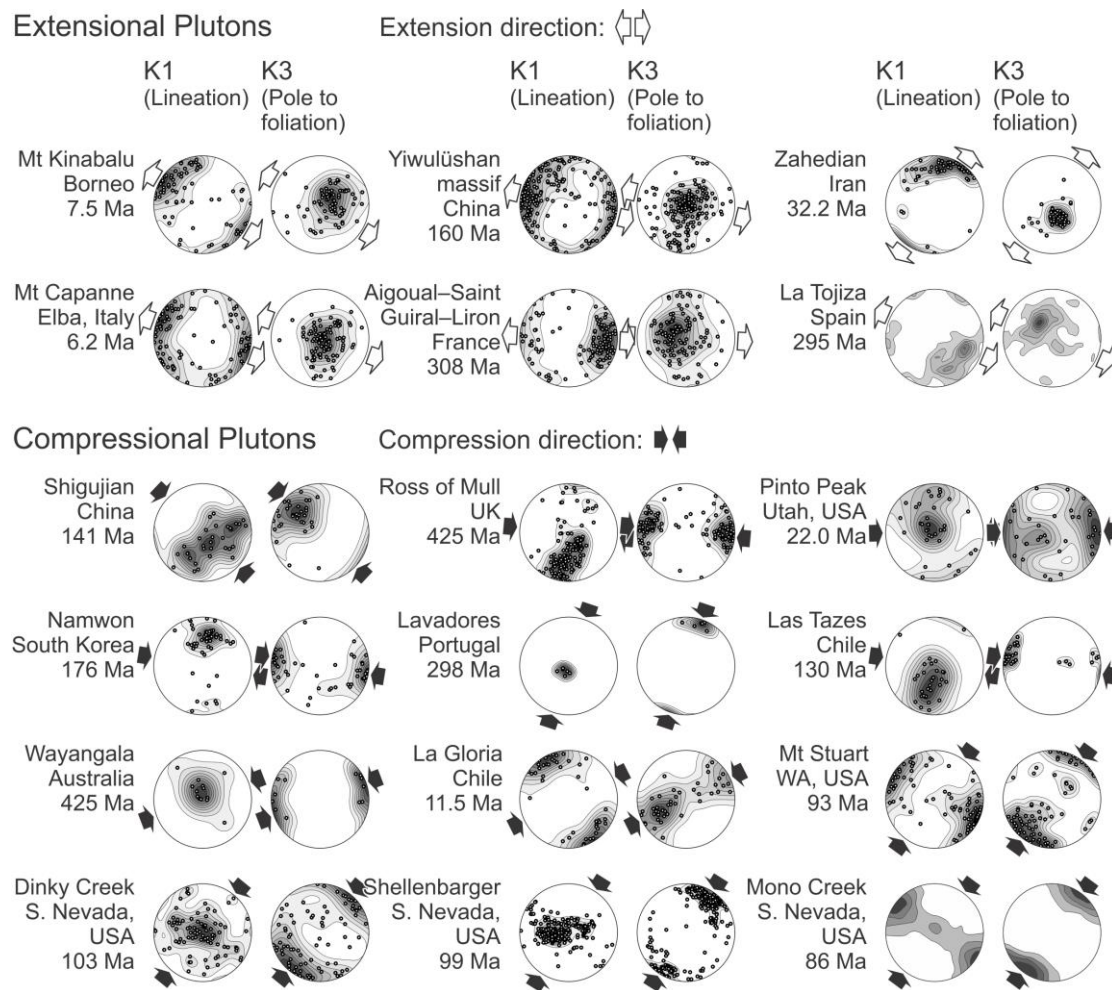
784



785

786 Fig. 10. Poles to planes for faults, aplite dykes and mafic dykes cross-cutting Mt
 787 Kinabalu (Burton-Johnson et al., 2017) compared to lineation (K1) and poles to
 788 foliation (K3) of the AMS fabric (excluding the Donkey Granite and Mesilau
 789 Porphyritic Granite). Open arrows illustrate the interpreted associated principal
 790 stress directions for structural data. Diamonds indicate maximum eigenvectors.

791

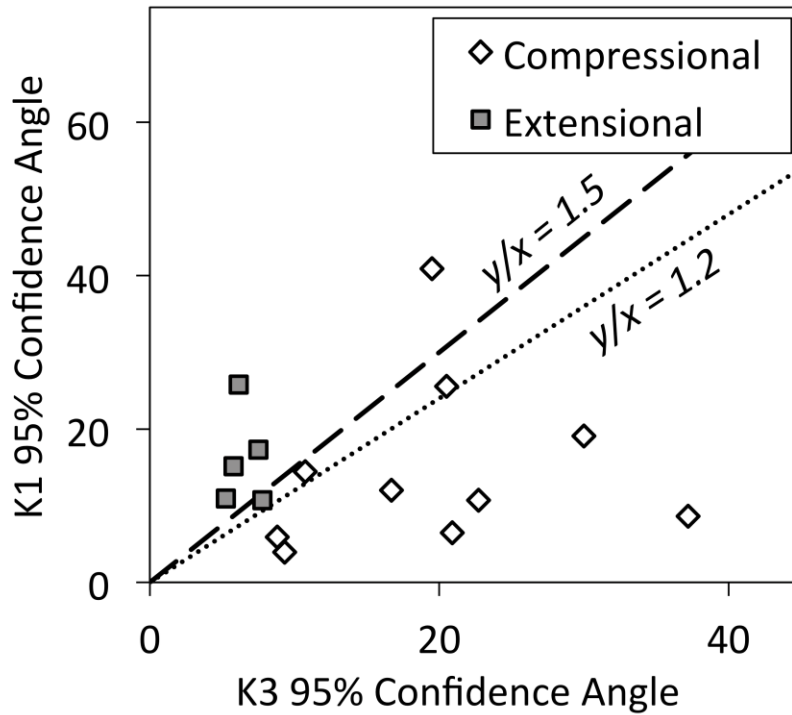


792

793 Fig. 11. Global compilation of lineation (K1) and pole to foliation (K3) directions
 794 of AMS data from intrusions emplaced in both extensional and compressive
 795 tectonic settings showing the orientation of the principal extensional or
 796 compressional direction generating the tectonic fabric.

797 Mt Kinabalu, Borneo – This study; Yiwulüshan massif - Lin et al. (2013); Zahedian
 798 - Sadeghian et al. (2005); Monte Capanne - Bouillin et al. (1993); Aigoual-Saint
 799 Guiral-Liron - Talbot et al. (2005); La Tojiza - Aranguren et al. (2003); Shigujian -
 800 Deng et al. (2013); Ross of Mull - Petronis et al. (2012); Pinto Peak - Petronis and
 801 O’Driscoll (2013); Namwon - Otoh et al. (1999); Lavadores - Martins et al. (2011);
 802 Las Tazes - Wilson (1998); Wyangala - Lennox et al. (2016); La Gloria - Gutiérrez
 803 et al. (2013); Mt Stuart - Benn et al. (2001); Dinky Creek - Cruden (1999);
 804 Shellenbarger - Tomek et al. (2017); Mono Creek - de Saint Blanquat and Tikoff
 805 (1997).

806



807

808 Fig. 12. 95% symmetrical confidence limits of the mean spherical K1 and K3 vector
 809 for the compressional and extensional plutons in Fig. 11. Compressional plutons
 810 can be identified at 90% confidence where “K1 95% Confidence Angle / K3 95%
 811 Confidence Angle” <1.2, and extensional plutons can be identified at 90%
 812 confidence where “K1 95% Confidence Angle / K3 95% Confidence Angle” >1.5.

813

Unit	Alexandra Tn/Gd	Low's Gt	King Gt	Donkey Gt	Paka Pph	Mesilau Pph
U-Pb Age (Ma)	7.85 ±0.08	7.69 ±0.07 - 7.64 ±0.11	7.46 ±0.08 - 7.44 ±0.09	7.46 > t > 7.32	7.32 ±0.09 - 7.22 ±0.07	- -
Approx. Vol. (Km ³)	0.2	2 (W) 4 (N)	90	0.4	40	40
SiO ₂ (wt. %)	61-65	59-64	62-66	63-65	63-67	60-65
Mg#	47-52	50-53	44-53	43-50	44-47	44-47
Phases (Modal %)						
Qz	23-28	16-28	14-27	23	15-21	7-21
Pl	40-45	25-33	21-38	26	23-33	24-28
Kfs	4-7	18-29	26-36	25	23-35	38-48
Hb	4-13	21-28	9-21	11	11-24	8-23
Bt	9-19	4-7	0-5	13	1-2	0-5
Cpx	-	-	-	-	-	0-2
Accessory	Ap, Ep	Ap, Ep, Zrn	Ap, Ep, Zrn	Ap	Ap	Ap, Spn

814

815 Table 1. Summary of U-Pb zircon ages (Cottam et al., 2010), SiO₂ and Mg# (Burton-
816 Johnson et al., in review), estimated volumes and modal mineralogies (Burton-
817 Johnson et al., 2017) of the major granitoid units. Abbreviations used: Tn –
818 Tonalite; Gd – Granodiorite; Gt – Granite; Pph – Porphyritic Granite; Qz – Quartz;
819 Pl – Plagioclase; Kfs – Potassium Feldspar; Hb – Hornblende; Bt – Biotite; Cpx. –
820 Clinopyroxene; Ap – Apatite; Ep – Epidote; Zrn – Zircon; Spn – Sphene (Whitney
821 and Evans, 2010).